

Nonlinear skin modes and fixed-points

C. Yuce

*Department of Physics, Eskişehir Technical University, Eskişehir 26555, Türkiye**

(Dated: November 20, 2024)

We investigate a one-dimensional tight-binding lattice with asymmetrical couplings and various type of nonlinearities to study nonlinear non-Hermitian skin effect. Our focus is on the exploration of nonlinear skin modes through a fixed-point perspective. Nonlinearities are shown to have no impact on the spectral region in the semi-infinite system; however, they induce considerable changes when boundaries are present. The spectrum under open boundary conditions is found not to be a subset of the corresponding spectrum under the semi-infinite boundary conditions. We identify distinctive features of nonlinear skin modes, such as power-energy dependence, degeneracy, and power-energy discontinuity. Furthermore, we demonstrate that a family of localized modes that are neither skin nor scale-free localized modes is formed with the introduction of a coupling impurity. Additionally, we show that an impurity can induce discrete dark and anti-dark solitons.

I. INTRODUCTION

The non-Hermitian skin effect leads to a large number of localized modes at the boundaries of the lattice, which is not possible in its Hermitian counterpart [1–4]. This effect can change both the spectral and dynamical properties of a system, giving rise to intriguing dynamical effects such as topological funneling and edge bursts [5–7]. Scale-free localization is another unique localization phenomena in non-Hermitian systems [8, 9]. This type of localization is different from both skin and Anderson localization as it implies size-dependent localization lengths [10, 11]. Scale-free localization challenges conventional understanding of localization concepts [12–19]. We note that even a single non-Hermitian defect in an otherwise Hermitian lattice can induce many localized modes whose localization lengths scale with system size [20, 21].

The non-Hermitian skin effect has been extensively studied, but only few papers extending this effect into the nonlinear regime have appeared in the literature [22–31]. For instance, we explored the nonlinear skin effect and constructed nonlinear skin modes, and discussed fractal structure [22]. M. Ezawa further extended the understanding of this effect by investigating dynamical nonlinear higher-order skin effect and identified a novel topological phase [24]. Experimental evidence of anomalous single-mode lasing, driven by the combined effects of nonlinearity and non-Hermiticity, was provided in [25]. Recent studies have analyzed the nonlinear perturbations of systems with high-order exceptional points, uncovering skin discrete breathers and hierarchical power-law scaling behaviors [26, 27]. In addition to these developments, ref. [28] have explored the emergence of insensitive edge solitons in non-Hermitian topological lattices, which exhibit robustness against perturbations. Reference [29] introduced the concept of solitons with self-induced topological nonreciprocity. An experimental demonstration of the nonlinear non-Hermitian skin effect and skin solitons in an optical system with Kerr nonlinearity has recently been realized [30].

The paper investigates the unique properties and behav-

iors of nonlinear skin modes in a generalized nonlinear system. We show that fixed points provides us construct nonlinear skin modes and its spectral regions for a finite size lattice and seminfinite lattice. We then outline the key similarities and differences between linear and nonlinear skin modes. Furthermore, we show that a coupling impurity induces a family of localized modes that are neither skin nor scale free localized modes, and also a discrete dark and anti-dark solitons.

II. MODEL

We start with the equation for the field amplitude ψ_n with $n = 1, 2, \dots, N$, describing 1D tight-binding nonlinear lattices with asymmetric couplings J_L and J_R

$$(1 + \alpha |\psi_n|^2) (J_L \psi_{n+1} + J_R \psi_{n-1}) + \left(\frac{g_1 |\psi_n|^2}{1 + \beta |\psi_n|^2} + g_2 |\psi_n|^4 + g_3 \psi_n^6 \right) \psi_n = E \psi_n \quad (1)$$

where α and β are either 0 or 1, $g_{1,2,3}$ are all real valued constants, and E is referred as energy for convenience. We set $J_L = 1$ and $J_R = \gamma$ with $0 \leq \gamma < 1$ for simplicity. Eq. (1) specifically describes a system with Kerr-type nonlinearity when $\alpha = \beta = g_2 = 0$, as well as other interesting nonlinearities such as saturable nonlinearity when $\alpha = g_2 = g_3 = 0$, Ablowitz-Ladik nonlinearity when $\beta = g_1 = g_2 = g_3 = 0$, and cubic-quintic-sextic nonlinearity when $\alpha = \beta = 0$, among others. We analyze this generalized equation under the following boundary conditions: $\psi_{N+1} = \psi_0 = 0$ for open boundary conditions (OBC) and $\psi_{N+1} = \psi_1, \psi_0 = \psi_N$ for periodic boundary conditions (PBC), and $\psi_\infty = \psi_0 = 0$ for the semi-infinite boundary conditions (SIBC). We refer to the SIBC and OBC spectra as the set of values that the parameter E can take for stable skin modes under SIBC and OBC, respectively.

Nonlinear systems exhibit two important features: chaos and fixed points, both of which can be explored in our system using an iterative approach. Starting with arbitrary initial values ψ_1 and E in Eq. (1), we iteratively compute the subsequent terms $\{\psi_2, \psi_3, \dots, \psi_{N+1}\}$

numerically, and then check if ψ_{N+1} satisfies the required boundary condition. For this reason, we discard solutions where ψ_n diverges and consider only bounded solutions. In the latter case, we see either chaotic behavior or fixed points, depending on the values of ψ_1 and E . Chaos arises when a slight variation in E leads to unpredictable behavior as n increases. In contrast, ψ_n may converge to a final value, known as the fixed point. This allows us to construct physically acceptable solutions. To find the fixed point, we require that ψ_n does not change with n when $n > N_c$, i.e., $\psi_{N_c+1} = \psi_{N_c+2} = \psi_{N_c+3} = a_0 e^{i\theta}$ in Eq. (1), where a_0 is a real number and θ is an arbitrary parameter. It is worth noting that the critical size N_c becomes a finite number at certain values of ψ_1 and E . However, determining these values as a function of the nonlinear parameters is challenging. The equation for a_0 reads

$$\left(\frac{g_1 a_0^2}{1 + \beta a_0^2} + g_2 a_0^4 + g_3 a_0^6\right) a_0 = (E - (1 + \alpha a_0^2) E_c) a_0 \quad (2)$$

where $E_c = 1 + \gamma$. This equation yields two types of solutions: the zero fixed point with $a_0 = 0$ and nonzero ones with $a_0 \neq 0$ being an E -dependent real solution of Eq. (2). Note that these fixed points are stable within a specific energy interval. Intriguingly, regardless of the nonlinear interaction strengths, the zero fixed point is stable for the semi-infinite system when E is enclosed by the linear PBC loop in the complex energy plane (defined by $E_{PBC} = e^{ik} + \gamma e^{-ik}$ with $-\pi \leq k < \pi$). This can be demonstrated through a linear stability analysis, where a small perturbation is introduced to ψ_n in Eq. (1) for $n > N_c$: $\psi_n \rightarrow a_0 e^{i\theta} + \epsilon \phi_n$ with $|\epsilon| \ll 1$ and $\phi_{N_c} = \phi_\infty = 0$. By omitting terms of order $|\epsilon|^2$ and higher, we see that the resulting equation does not include any nonlinear parameters when $a_0 = 0$ ($\phi_{n+1} + \gamma \phi_{n+1} = E \phi_n$), indicating that ϕ_n become exactly the linear SIBC eigenstates whose energies are inside the linear PBC loop. Beyond this energy region, it becomes unstable as ϕ_n diverges. It is interesting to see that the zero fixed point loses its stability in the Hermitian case with $\gamma = 1$, as the eigenstates ϕ_n become extended, causing the zero fixed point to shift to a nonzero value. This explains why nonlinear skin modes are unique to the non-Hermitian system with $\gamma \neq 1$. In this paper, we use these fixed points to construct skin and extended modes, since $a_0 = 0$ and $a_0 \neq 0$ ensure SIBC (or OBC when N_c is finite) and PBC, respectively [33].

The fixed point can also be studied in a bifurcation diagram. For clarity and simplicity, we present a bifurcation diagram for the system with only Kerr-type nonlinearity and real valued ψ_1 and E (note that $\psi_1 \rightarrow \psi_1 e^{i\theta}$ leaves E unaffected and transforms ψ_n to $\psi_n e^{i\theta}$). Fig. 1(a) shows it for positive real values of E at $\gamma = 0.2$ and $g_1 = 1$. The field amplitude always collapses to zero for $E < E_c = 1.20$, and converges to an E -dependent nonzero value until E reaches 2.37, where the nonzero fixed point (period one orbit) becomes unstable, and period-2 points occur, where ψ_n starts to alternate between two values

instead of converging to a single number. Similarly, at a higher value of E , the period-2 points lose stability and bifurcate into period-4 points. This period-doubling behavior continues to period-8, 16 points, etc. until the system exhibits chaotic behavior at $E = 2.65$, where a tiny variation in E can lead to a non-periodic behavior in the field amplitude. In this case, the solutions become incompatible with the boundary conditions. The iteration eventually diverges when $E \geq 2.78$.

Let us now construct extended and skin modes based on the bifurcation diagram in Fig. 1(a). One can obtain extended PBC modes at period-1, period-2, and higher periods until the system enters the chaotic regime, where ψ_n no longer converges to a nonzero fixed point. For example, at a period-2 point occurring at $E = 2.37$, one can obtain extended modes by setting the initial value ψ_1 to either of these two values to satisfy PBC. In this case, ψ_j oscillates between these two values, causing the corresponding density to exhibit a sawtooth shape, in contrast to the uniform density of the extended modes with a period of 1. Similarly, at a period-4 point, extended modes oscillate between four distinct values, as shown in the inset of Fig. 1(a). Consider next $E < E_c$. In this case, skin modes localized at the left edge appear as ψ_n converges to the zero fixed point, satisfying SIBC (and also OBC when N_c is finite). As an illustration, we plot the densities of the skin modes up to $n = 100$ at $\psi_1 = 0.1$ and $\psi_1 = 0.3$, and two different energies in Fig. 1(b). This plot shows how quickly the field amplitude approaches zero and then gradually decreases to zero, even if N_c is infinite. Therefore, such SIBC skin modes may practically be regarded as quasi-stationary OBC modes that maintain their forms over an extended period of time in sufficiently long lattices, as they approximately satisfy OBC [31, 32]. It is worth noting that the localization lengths of the skin modes remain constant with system size but increase with energy E , similar to those observed in the linear model. However, the form of the skin modes depends on the power ($P = \sum_{n=1}^N |\psi_n|^2$), as illustrated in the Fig. 1(b), where ψ_1 is varied from 0.1 to 0.3, leading to tighter localization. Note that the power under this change in ψ_1 increases by a factor of nearly 7 and 6 at $E = 1$ and $E = 1.1$, respectively. It is important to mention that such a scaling of ψ_1 at fixed E does not generate a distinct skin mode in the linear system. To this end, we note that increasing γ extends the skin modes further from the left edge. Our extensive numerical computations across various nonlinear parameters indicate that this extension reaches the lattice size at $\gamma = 1$, converting skin modes into extended ones, as illustrated in the inset of Fig. 1(b). This suggests that nonlinear OBC skin modes are unique to the non-Hermitian system, $\gamma \neq 1$, which is in agreement with our previous finding that the zero fixed point loses its stability at $\gamma = 1$.

A portion of SIBC skin modes with finite N_c are OBC skin modes, exhibiting novel features such as a continuous spectrum, degeneracies, and energy-power branches. To explore these characteristics, one may begin by itera-

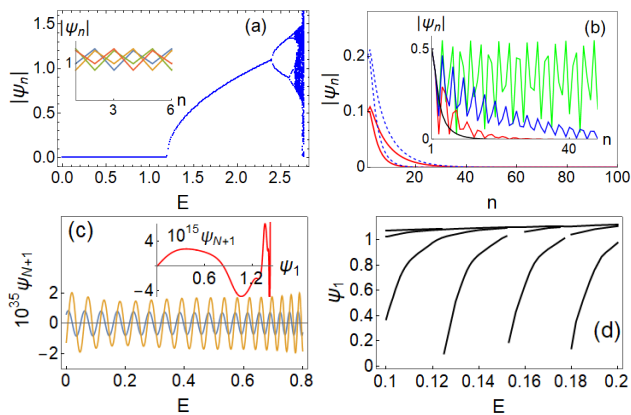


FIG. 1. (a) The bifurcation diagram reveals the critical value $E_c = 1.2$, below which the zero fixed point appears, and above which E -dependent fixed points arise. Period doubling occurs at $E = 2.37$, followed by chaos at $E = 2.65$. In the inset, the densities of the extended PBC modes at a period-4 point with $E = 2.6$ are illustrated up to $n = 6$. (b) $|\psi_n|$ for the skin modes when $\psi_1 = 0.1$ (solid red) and $\psi_1 = 0.3$ (dashed blue) at two different energies at $E = 1$ and $E = 1.1$ (the more extended ones) are shown. The inset demonstrates that the localization lengths of the skin modes with $\psi_1 = 0.5$ and $E = 1$ increase as γ is increased from 0.2 (in black) and 0.7 (in red) to 0.9 (in blue), eventually becoming equal to the lattice size at $\gamma = 1$ (in green), implying that skin modes are unique to the non-Hermitian systems. (c) The scaled field amplitude as a function of E when $\psi_1 = 0.6$ (in blue) and $\psi_1 = 0.9$ (in orange), and $N = 100$. The inset shows the scaled field amplitude at $E = 1$ and $N = 100$ as a function of ψ_1 , indicating that OBC is satisfied at certain values of ψ_1 . (d) The relation between E and ψ_1 for OBC modes with $N = 100$ in the E -interval $[0.1, 0.2]$. The common parameters are $\gamma = 0.2$ (except for the inset in (b)), $g = 1$ and all other nonlinear interaction strengths are zero.

tively computing ψ_{N+1} as a function of E for an arbitrary value of ψ_1 , and then determine the values of E at which OBC is satisfied, i.e., $\psi_{N+1}(E) = 0$. For an illustration, Fig. 1(c) plots the scaled field amplitudes as a function of E at $\psi_1 = 0.6$ and $\psi_1 = 0.9$ when $N = 100$. As can be seen, they oscillate between negative and positive values as E increases and touch zero at certain values of E . These specific values, where $\psi_{N+1} = 0$, correspond to OBC skin modes. As can be seen, selecting a different arbitrary value for ψ_1 generates distinct value of E , so varying ψ_1 continuously generates a continuum of E . Secondly, to illustrate that two or more distinct OBC skin modes can share the same value of E but have different powers, let us fix E and plot ψ_{N+1} as a function of ψ_1 . As shown in the inset of Fig. 1(c), $\psi_{N+1} = 0$ at more than one value of ψ_1 , implying degeneracy as distinct OBC skin modes exist at the same value of E , each with a different power (correspondingly different ψ_1). Finally, the modes display an additional characteristic: the energy-power branches. We perform numerical calculations to determine the relation between E and ψ_1 when $0.1 \leq E \leq 0.2$. Fig. 1(d) reveals non-smooth behavior be-

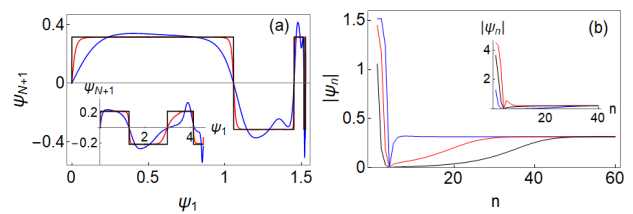


FIG. 2. (a) The condition $\psi_{N+1} = 0$ is satisfied at specific points that are very close to each other for different lattice sizes: $N = 5$ (blue), $N = 10$ (red), and $N = 100$ (black). (b) ψ_n for 3 different ψ_1 up to $n = 60$ show that the field amplitude takes zero value (at $n = 4$) before reaching a nonzero fixed point. This means that OBC modes are available at $N = 3$, but the SIBCs are not at this energy. The common parameters are $E = 1.3 > E_c$, $\gamma = 0.2$, and $g_1 = 1$ (only Kerr-type nonlinearity). For the insets, the nonlinear strengths are $\alpha = \beta = g_1 = 20g_2 = 1$, $g_3 = 0$

tween E and ψ_1 . This novel type of branched structure is characterized by dramatic changes in the lowest possible values of ψ_1 at certain energies, implying that the powers for the OBC skin modes exhibit discontinuities in E . For example, an OBC mode is available at $\psi_1 = 0.10$ when $E = 0.125$, whereas it appears at $\psi_1 = 0.98$ when E is just below this value.

The SIBC spectra for both the linear and nonlinear systems fill the same disk, bounded by the linear PBC loop in the complex energy plane, but the corresponding OBC spectra do not share this similarity. In the linear system, the OBC spectrum is confined to the interval of $\mp 2\sqrt{\gamma}$ on the real energy axis, with its width ($4\sqrt{\gamma}$) being independent of the system size, implying that it is a subset of the corresponding SIBC spectrum. However, in the nonlinear case, OBC spectrum is intriguingly not bounded by the SIBC spectrum and its width decreases with increasing lattice size, eventually approaching that of the SIBC on the real energy axis. In other words, OBC skin modes exist with energy E outside the range defined by $\mp E_c$. The key factor behind this intriguing behavior is that, for either $E > E_c$ or $E < -E_c$, ψ_n initially decays and becomes zero at a certain point n_0 (satisfying OBC for the system with $N = n_0 - 1$) but then slowly increases to a nonzero fixed point and remains at that fixed point, violating SIBC. Fig. 2(a) confirms this by presenting ψ_{N+1} as a function of ψ_1 at $E = 1.3 > E_c$ for three different system sizes. We see that OBCs are satisfied at specific values of ψ_1 , which are almost the same for the three lattice sizes (indistinguishable by the naked eye in the figure). Fig. 2(b) shows the density plots for some values of ψ_1 , revealing that OBC is satisfied at $N = 3$, whereas SIBC is not, as the field amplitude reaches a fixed point at large values of n . To this end, we would like to say that N_c does not take finite values when E is complex, suggesting that the nonlinear OBC spectrum is real valued, similar to the linear OBC spectrum.

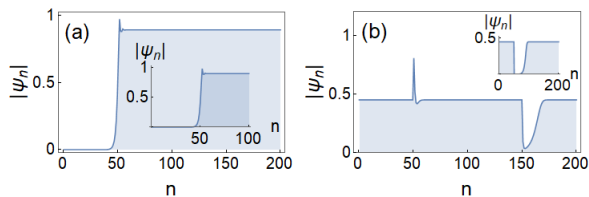


FIG. 3. (a) $|\psi_n|$ for the localized OBC modes in the presence of a single coupling impurity at the edge when $W_1 = 1$, $\psi_1 = 10^{-14}$, $E = 2$ and $N = 200$ ($N = 100$ in the inset). (b) The dark and anti-dark soliton under PBC in the system with $\psi_1 = 0.447$, $3p = p' = 150$, $W_2 = -W_1 = 0.8$ and $E = 1.4$. The width of the dark soliton can be increased by placing the second impurity next to the first one (see the inset at $p = p' - 1 = 50$, and $W_1 = 1$ and $W_2 = -0.2002$). The common parameters are $\gamma = 0.2$ and $g_1 = 1$.

III. IMPURITY INDUCED MODES

In the linear non-Hermitian lattice, a coupling impurity may induce an extensive number of scale-free localized states whose localization lengths scale with the system size. Here, we show that in the nonlinear case, it may lead to the formation of unique localized modes, as well as dark solitons.

Let us introduce a coupling impurity with strength W_1 at site p such that J_R in Eq. (1) is modified to $J_R \rightarrow \gamma + W_1\delta_{n,p}$ ($J_L = 1$). Consider $E > E_c$, where ψ_n converges to a nonzero fixed value. When the impurity with an appropriate strength is introduced at the right edge, it cause the field amplitude to drop to zero value from the nonzero fixed point at that edge. Conversely, when the impurity is located in the bulk, it perturbs the field amplitude around itself, while the field amplitude away from the impurity in both directions is equal to the nonzero fixed point. The former one may lead to localized modes, while the latter one to dark solitons.

We start with the case where the impurity is located at the right edge. Since the initial value ψ_1 does not change the nonzero fixed point, we propose assuming a very small value for ψ_1 , such as $\psi_1 < 10^{-10}$. In this case, the field amplitude is practically zero near the left edge, and reaches the nonzero fixed value away from the left edge, and remains constant towards the right edge, thus allowing us to construct localized modes at the right edge. Note that the OBC is satisfied with an appropriate choice of the impurity strength W_1 . As the nonzero fixed value varies with E , a family of localized modes is generated until E becomes sufficiently large for the system to enter into a chaotic regime. As an illustration, Fig. 3(a) plots $|\psi_n|$ when $N = 200$ and $\psi_1 = 10^{-14}$. Notably, the specific lattice site where the field amplitude reaches the nonzero fixed value remains the same regardless of the system size as can be seen in the inset in Fig. 3(a) for $N = 100$. Therefore, these modes are neither skin nor scale free localized modes whose localization lengths remain constant or change proportionally with the system

size, respectively.

A single coupling impurity may also lead to dark or anti-dark soliton solutions under PBC. A dark (anti dark) soliton is a localized drop (increase) in the density on the uniform background. To obtain them, we place the impurity in the bulk and perform the iteration with $\psi_1 = a_0$ (period one orbit) and the corresponding energy such that the extended PBC state with uniform density would be obtained in the absence of the impurity. Therefore, the field amplitude at the left side of the impurity is not changed: $\psi_n = a_0$ when $n < p$. However, the field amplitude will either increase or dip at the impurity location, depending on the sign of W_1 , and then returns to the fixed point after a few lattice sites, remaining constant towards the right edge. In this way, we obtain dark solitons when $W_1 > 0$ and anti-dark solitons when $W_1 < 0$. Additionally, if the system contains two well-separated impurities at sites p and p' with opposite strengths, $W_2 = -W_1$, we can generate a pair of dark and anti-dark solitons, as illustrated in Fig. 3 (b). Introducing additional well-separated impurities into the system allows for the formation of multiple dark and anti-dark solitons. On the other hand, placing the two impurities on neighboring lattice points, $p' = p \mp 1$, allows us to adjust both the dip point and the width of the dark soliton. As shown in the inset in Fig. 3 (b), the density drops to zero at the impurity position and then returns to its fixed point after a certain distance, leading to a wider dark soliton. Adding more neighboring impurities allows us to obtain much wider dark solitons.

IV. CONCLUSIONS

Non-Hermitian skin effect is crucial as it reveals unique localization phenomena that has no Hermitian counterpart, and extending this effect to the nonlinear domain is essential for investigating its potential applications in advanced material science with enhanced performance, such as sensors, waveguides, or filters, where controlling or exploiting nonlinearity is advantageous. In this work, we explore a generalized nonlinear equation and show that zero fixed points can provide a framework for deriving nonlinear skin modes. We also discuss that the zero fixed point loses its stability and the nonlinear skin modes disappear when the system has no asymmetrical couplings, i.e., when the system is Hermitian. It is intriguing to find that the spectra of both linear and nonlinear skin modes under SIBC occupy the same disk, bounded by the linear PBC loop in the complex energy plane. However, the spectral region of the OBC skin modes is significantly altered by the nonlinear interaction. Furthermore, the OBC spectrum is not a subset of the corresponding SIBC spectrum. The nonlinear OBC skin modes are power-dependent, and a continuum of energies associated with OBC skin modes appear, in contrast to the discrete energies for the linear system. Additionally, two or more distinct nonlinear OBC skin modes can share the same

energy. Introducing a single coupling impurity may lead to dark or anti dark soliton solutions under PBC, and localized modes that are neither skin nor scale free localized modes under OBC.

This study was supported by Scientific and Technological Research Council of Turkey (TUBITAK) under the grant number 124F100. The authors thank to TUBITAK for their supports.

* cyuce@eskisehir.edu.tr

- [1] Shunyu Yao and Zhong Wang, “Edge states and topological invariants of non-hermitian systems”, *Phys. Rev. Lett.* **121**, 086803 (2018).
- [2] Huitao Shen, Bo Zhen, and Liang Fu, “Topological Band Theory for Non-Hermitian Hamiltonians”, *Phys. Rev. Lett.* **120**, 146402 (2018).
- [3] Nobuyuki Okuma, Kohei Kawabata, Ken Shiozaki, and Masatoshi Sato, “Topological Origin of Non-Hermitian Skin Effects”, *Phys. Rev. Lett.* **124**, 086801(2020).
- [4] Kai Zhang, Zhesen Yang, and Chen Fang, “Correspondence between Winding Numbers and Skin Modes in Non-Hermitian Systems”, *Phys. Rev. Lett.* **125**, 126402 (2020).
- [5] S. Weidemann, M. Kremer, T. Helbig, T. Hofmann, A. Stegmaier, M. Greiter, R. Thomale, A. Szameit, “Topological funneling of light”, *Science* **6488**, 311 (2020).
- [6] Z. Turker and C. Yuce, “The funneling effect in a non-Hermitian Anderson Model”, *Phys. Scr.* **99**, 075028 (2024).
- [7] C. Yuce and H. Ramezani, “Non-Hermitian edge burst without skin localization”, *Phys. Rev. B* **107**, L140302 (2023).
- [8] Linhu Li, Ching Hua Lee, Jiangbin Gong, “Impurity induced scale-free localization”, *Communications Physics* **4**, 42 (2021).
- [9] L. Li, C. H. Lee, S. Mu, and J. Gong, “Critical non-Hermitian skin effect”, *Nat. Commun.* **11**, 5491 (2020).
- [10] Bo Li, He-Ran Wang, Fei Song, and Zhong Wang, “Scale-free localization and PT symmetry breaking from local non-Hermiticity”, *Phys. Rev. B* **108**, L161409 (2023).
- [11] Cui-Xian Guo, Xueliang Wang, Haiping Hu, and Shu Chen, “Accumulation of scale-free localized states induced by local non-Hermiticity”, *Phys. Rev. B* **107**, 134121 (2023).
- [12] Paolo Molignini, Oscar Arandes, Emil J. Bergholtz, “Anomalous skin effects in disordered systems with a single non-Hermitian impurity”, *Phys. Rev. Research* **5**, 033058 (2023).
- [13] Kazuki Yokomizo, Shuichi Murakami, “Scaling rule in critical non-Hermitian skin effect”, *Phys. Rev. B* **104**, 165117 (2021).
- [14] S. M. Rafi-Ul-Islam, Zhuo Bin Siu, Haydar Sahin, Ching Hua Lee, and Mansoor B. A. Jalil, “Critical hybridization of skin modes in coupled non-Hermitian chains”, *Phys. Rev. Research* **4**, 013243 (2022).
- [15] Wei Li, Zhoujian Sun, Ze Yang, and Fuxiang Li, “Universal scalefree non-Hermitian skin effect near the Bloch point”, *Phys. Rev. B* **109**, 035119 (2024).
- [16] Fang Qin, Ye Ma, Ruizhe Shen, and Ching Hua Lee, “Universal competitive spectral scaling from the critical non-Hermitian skin effect”, *Phys. Rev. B* **107**, 155430 (2023).
- [17] He-Ran Wang, Bo Li, Fei Song and Zhong Wang, “Scale-free non-Hermitian skin effect in a boundary-dissipated spin chain”, *SciPost Phys.* **15**, 191 (2023).
- [18] Xinrong Xie, et. al., “Observation of scale-free localized states induced by non-Hermitian defects”, *Phys. Rev. B* **109**, L140102 (2024).
- [19] Yongxu Fu, Yi Zhang, “Hybrid scale-free skin effect in non-Hermitian systems: A transfer matrix approach”, *Phys. Rev. B* **108**, 205423 (2023).
- [20] Cui-Xian Guo, Chun-Hui Liu, Xiao-Ming Zhao, Yanxia Liu, and Shu Chen, “Exact Solution of Non-Hermitian Systems with Generalized Boundary Conditions: Size-Dependent Boundary Effect and Fragility of the Skin Effect”, *Phys. Rev. Lett.* **127**, 116801 (2021).
- [21] Linhu Li, Ching Hua Lee, Sen Mu, Jiangbin Gong, “Critical non-Hermitian Skin Effect”, *Nat. Commun.* **11**, 5491 (2020).
- [22] C. Yuce, “Nonlinear non-Hermitian skin effect”, *Phys. Lett. A* **408**, 127484 (2021).
- [23] S. Tombuloglu, C. Yuce, “Nonlinear waves in an anti-Hermitian lattice with cubic nonlinearity *Commun. Nonlinear Sci. Numer. Simulat.* **83**, 105106 (2020).
- [24] Motohiko Ezawa, “Dynamical nonlinear higher-order non-Hermitian skin effects and topological trap-skin phase”, *Phys. Rev. B* **105**, 125421 (2022).
- [25] Bofeng Zhu, et. al., “Anomalous Single-Mode Lasing Induced by Nonlinearity and the Non-Hermitian Skin Effect”, *Phys. Rev. Lett.* **129**, 013903 (2022).
- [26] Hui Jiang, Enhong Cheng, Ziyu Zhou and Li-Jun Lang, “Nonlinear perturbation of a high-order exceptional point: Skin discrete breathers and the hierarchical power-law scaling”, *Chin. Phys. B* **32**, 084203 (2023).
- [27] Bertin Many Manda, Ricardo Carretero-Gonzalez, Panayotis G. Kevrekidis, and Vassos Achilleos, “Skin modes in a nonlinear Hatano-Nelson model”, *Phys. Rev. B* **109**, 094308 (2024).
- [28] Bertin Many Manda, Vassos Achilleos, “Insensitive edge solitons in non-Hermitian topological lattices”, arXiv:2405.05441.
- [29] Pedro Fittipaldi de Castro, Wladimir Alejandro Benalcazar, “Solitons with Self-induced Topological Nonreciprocity”, arXiv:2405.14919.
- [30] Shulin Wang, et. al., “Nonlinear Non-Hermitian Skin Effect and Skin Solitons in Temporal Photonic Feedback Lattices”, arXiv:2409.19693.
- [31] H. Ghaemi-Dizicheh, “A class of stable nonlinear non-Hermitian skin modes”, arXiv:2407.08880.
- [32] C. Yuce, H. Ramezani, “Stabilization of zero-energy skin modes in finite non-Hermitian lattices”, *Phys. Rev. A* **106**, 063501 (2022).
- [33] $|\psi_n|$, rather than ψ_n itself, can converge to a fixed value. However, this approach doesn’t provide insights into the behavior of nonlinear skin modes, but rather addresses extended modes.